6 Modeling Methods for Prediction of Asphaltene Deposition

N. R. Babu, P. Lin, J. Zhang, M. Tavakkoli, and F. M. Vargas

CONTENTS

6.1 Asphaltene Deposition in Wellbore and Pipelines 204
6.1.1 Modeling Asphaltene Deposition 204
6.1.1.1 Initial Works 204
6.1.1.2 Models Based on Capillary-Deposition Tests 205
6.1.1.3 Models Based on Deposition Tests in New Geometries 206
6.1.2 Development of Asphaltene Deposition Tool 207
6.1.2.1 Assumptions 209
6.1.2.2 Model Development 209
6.1.3 Modeling Asphaltene Aggregation 214
6.2 Asphaltene Deposition in Porous Media 217
6.2.1 Deposition Models for Porous Media 217
6.2.2 Introduction to Lattice Boltzmann Modeling 220
6.2.2.1 Distribution Function 221
6.2.2.2 Boltzmann Transport Equation 222
6.2.2.3 The BGK Model 222
6.2.2.4 Lattice Arrangement 222
6.2.3 Application of LBM 223
6.2.3.1 Assumptions 224
6.2.3.2 Model Development 224
6.3 Modeling of Asphaltene-Transport Properties 227
6.3.1 Density 227
6.3.2 Viscosity 228
6.3.2.1 Lohrenz-Bray-Clark (LBC) Method 228
6.3.2.2 Friction Theory 230
6.3.2.3 Corresponding State Principle Models 231
6.3.2.4 Effect of Asphaltene Precipitation on Apparent Viscosity of Oil 235
6.3.3 Diffusion Coefficient 236
6.4 Final Remarks 237
References 237

The potential for asphaltene to precipitate and deposit in wellbore and flow lines as a result of changes in pressure, temperature, and composition of crude oil is a major concern for the oil-and-gas industry. Asphaltene-deposit removal from onshore and offshore facilities is an expensive operation. To properly assess the risk of asphaltene deposition, experimental and modeling techniques have been developed to predict the asphaltene-deposition profile and rate. There have been only a few established works on modeling asphaltene deposition in wellbores and pipelines as well as in porous media compared with the number of works dedicated to the development of thermodynamic models to investigate asphaltene precipitation. It is important to establish an efficient and reliable modeling technique to understand the mechanism of asphaltene deposition in the oil field based on the various laboratory-scale experimental results.

Several experimental techniques developed to study asphaltene deposition at different pressure and temperature conditions and flow regimes were presented in Chapter 5. In this chapter, modeling methods for the prediction of asphaltene deposition, developed over the years, will be discussed. Asphaltene-deposition modeling in wellbores and pipelines has been investigated by researchers for only the last few years. Although asphaltene deposition in porous media has been studied for a relatively longer period of time, this is still an area of active research to achieve a simple, yet comprehensive model that can capture the relevant physics of asphaltene-deposition phenomena.

6.1 ASPHALTENE DEPOSITION IN WELLBORE AND PIPELINES

6.1.1 Modeling Asphaltene Deposition

6.1.1.1 Initial Works

A multiphase multicomponent hydrodynamic model was proposed by Ramirez-Jaramillo et al. (2006) to represent the asphaltene-deposition phenomenon in production wells. Molecular diffusion and shear removal were considered as the two competing mechanisms that define the radial diffusion and later the deposition of asphaltenes. Particle transport toward the wall was considered to be caused by temperature gradient at the wall. This modeling approach was based on the well-developed theory of wax deposition (Burger et al. 1981). But this theory and modeling approach for asphaltene deposition were not supported by experimental results obtained using the organic solid deposition and control device (OSDC). The experimental method to analyze asphaltene deposition using the OSDC was described in detail in Section 5.1.1.3. Based on the OSDC results, there was no pronounced effect of temperature gradient at the wall on the asphaltene-deposition rate (Akbarzadeh et al. 2009).

Soulgani et al. (2009) introduced an asphaltene-deposition model on the basis of a series of experiments on an externally heated stainless-steel pipe. These experiments were conducted to observe the role of various parameters such as oil-flow rate, temperature, and concentration of asphaltene precipitant on the rate of asphaltene deposition. The model for asphaltene deposition was developed based on the results

of these experiments. It was assumed that the deposition on the heated pipe surface is controlled by a chemical-reaction mechanism based on an Arrhenius exponential term. The asphaltene-deposition rate was fitted to a simple correlation, which included parameters such as temperature, velocity, and precipitated-asphaltene concentration. It was found that asphaltene deposition increases as temperature and concentration of precipitated-asphaltene particles increases. No solid proofs supporting the suggested deposition mechanism was provided.

6.1.1.2 Models Based on Capillary-Deposition Tests

The model developed by Vargas et al. (2010) is more advanced in comparison with the predecessors. Submodels describing particle precipitation, aggregation, transport, and deposition on the wall were included. The aggregation and the deposition phenomena were modeled using pseudo–first-order reactions. A deposition simulator was proposed based on species-conservation equations coupled with thermodynamic modeling of oil using the perturbed chain statistical associating fluid theory (PC-SAFT) equation of state (EoS), which was described in detail in Section 4.2.3.2. A competing phenomenon between aggregation and deposition was identified. The model contained three parameters that were estimated from experiments. The authors demonstrated that their model adequately describes the asphaltene deposition in capillary tubes. The effect of temperature on the deposition rate was also studied. It was showed that in a capillary, as temperature increases, the asphaltene-deposition flux increases toward the capillary inlet and rapidly decreases toward the outlet. This behavior was found to be in good agreement with experimental data obtained from capillary experiments.

The work done by Kurup et al. (2011) is a continuation of the deposition simulator developed by Vargas et al. (2010). It involved the development of an asphaltene deposition tool (ADEPT) that can predict the occurrence and calculate the magnitude and profile of asphaltene deposition in a wellbore. The simulator consisted of a thermodynamic module and a deposition module. PC-SAFT EoS was used in the thermodynamic module to describe the phase behavior of oil, which was first characterized by using thermodynamic properties such as saturation points, asphaltene onset pressure data, and physical properties such as the density of the oil (Section 4.2.3.2). The deposition module was then used along with input from the thermodynamic module to calculate the magnitude of asphaltene deposited along the length of the wellbore and pipelines. Similar to the model developed by Vargas et al. (2010), this deposition model also consisted of three tuning parameters, each for precipitation, aggregation, and deposition mechanisms. But instead of a two-dimensional convection-diffusion transport equation as in Vargas et al. (2010), this model was simplified to a one-dimensional axial-dispersion equation. The mathematical model used in the deposition module was first benchmarked and validated by comparing the simulation results against the experimentally measured asphaltene-deposition flux in a capillary deposition experiment, as illustrated in Section 5.1.1.1 (Wang et al. 2004; Kurup et al. 2012). The simulator was then used to study deposition in two field cases: Kuwait's Marrat oil well and Algeria's Hassi-Messaoud oil field (Kurup et al. 2012). A proper choice of the kinetic parameters helped the deposition

simulator in predicting the deposition profile both qualitatively and quantitatively, and the predictions matched very well with the field observations. It should be noted that the simulator does have limitations in capturing the entire physics of the deposition process because it is just a one-dimensional model. A detailed description of ADEPT is included in Section 6.1.2.

As discussed by Vargas et al. (2010) and Kurup et al. (2011) the transport of precipitated-asphaltene particles and their subsequent deposition on surfaces are described by the convection-diffusion equations. Because there is a lack of understanding of the rich physics involved in the deposition process, the transport model is frequently of a mechanistic nature, and it relies heavily on experimental data. A more rigorous analysis of the asphaltene-deposition model can be done using a computational fluid dynamic (CFD) approach. As asphaltene starts depositing on the wall surface of the wellbore or pipeline, its cross-section is continuously reduced, subsequently changing the flow field. Hence, it is important to track the deposition front while modeling asphaltene deposition. Ge et al. (2013) presented a general framework for modeling the asphaltene-deposition process that focuses on a CFD-based transport model with an evolving depositing front coupled to the associated fluid, mass, and energy transport. The deposition front was captured using either a level-set approach or a total-concentration approach. The deposition process occurring at the depositing front was modeled as a first-order reaction. Fluid flow was modeled using the incompressible Navier-Stokes equations.

Along similar lines, much recently, a one-dimensional model for asphaltene deposition in wellbores or pipelines was presented by Guan et al. (2017). This model consisted of the thermodynamic module and the transport module. The thermodynamic module focused on the modeling of asphaltene precipitation using the Peng-Robinson EoS (Section 4.2.3.1). The transport module included the modeling of fluid transport, particle transport, and asphaltene deposition while tracking the deposition front as well. Three parameters, each for precipitation, aggregation, and deposition kinetics, were required in this model. Although a reasonably accurate prediction of the asphaltene-deposit layer profile was attained, enhanced performance of the thermodynamic module could be attained by incorporating the PC-SAFT EoS.

6.1.1.3 Models Based on Deposition Tests in New Geometries

Eskin et al. (2011) developed a deposition model, accounting for major mechanisms of particle transport to the wall such as Brownian and turbulent diffusions, turbophoresis, and used-particle-flux mass-transfer expressions for turbulent flows to model the deposition process. The model parameters were obtained by fitting the model predictions to the deposition results obtained from RealView, which is an OSDC (Section 5.1.1.3). The model consisted of a submodel describing the particle-size distribution evolution in time in a Couette device and along a pipe and a submodel for calculating the particle transport to the wall. The concept of critical particle size was applied, where only particles that are smaller than the critical size can deposit, which is in agreement with the model proposed by Vargas et al. (2010). A shear-removal term was also introduced to account for the increased shear rate at the wall and decreased

deposit at higher speeds of the RealView cell. The model contained six parameters that are determined based on experiments in the RealView cell. Akbarzadeh et al. (2012) used this model and showed simulation results for asphaltene deposition with respect to experiments performed on various oils. The impacts of shear, run time, residence time, pressure, chemical inhibitor, and surface roughness on the deposition of asphaltenes were investigated. Also, for the developed asphaltene-deposition model, the number of parameters were reduced from six to two (for the oils under their study) by performing sensitivity analyses. Finally, the simulation results for deposition of asphaltenes in vertical production tubings were qualitatively compared with field observations reported by Haskett and Tartera (1965). A population balance model (similar to the one established by Maqbool et al. 2011 and as discussed in Section 6.1.3) was employed for modeling the asphaltene aggregation instead of a simple second-order reaction mechanism as in Kurup et al. (2012).

Recently, asphaltene deposition was measured using a packed-bed apparatus by Vilas Boas Fávero et al. (2016). It was showed that a mass-transfer-limited one-dimensional deposition model can explain the asphaltene deposition of nanometer-sized unstable asphaltenes in the viscous-flow regime. The model does not have any parameters to be tuned against the experimental data, but the mass-transfer coefficient is estimated using a simplified empirical correlation. Though this is the first work on such an apparatus, the model needs to be more comprehensive of the mechanisms taking place in the column. This demands a more-rigorous modeling approach and prediction technique for the simulation of asphaltene deposition in such a geometry.

The capabilities and limitations of the significant models reviewed in this section are summarized in Table 6.1.

6.1.2 Development of Asphaltene Deposition Tool

To comprehend the process of asphaltene deposition taking place in the wellbore and pipelines, a simple, yet comprehensive tool developed by Kurup et al. (2011) will be discussed in detail in this section.

At reservoir conditions, the asphaltenes are mostly stable and soluble in oil. However, a change in pressure, temperature, and composition makes the asphaltenes that are originally dissolved in the oil destabilized and leads to phase separation of asphaltenes from oil. These precipitated asphaltenes are known as *primary particles*. These primary particles then combine with each other to form aggregates. It is proposed that these primary particles are susceptible to deposit on the walls of the wellbore. Hence, the three steps that take place in the wellbore, namely, precipitation, aggregation, and deposition of asphaltenes, can be modeled using a transport (convection-diffusion) equation. Based on this notion, Vargas et al. (2010) developed a two-dimensional convection-diffusion deposition model. ADEPT is a modification of the Vargas et al. (2010) model. It is a simple one-dimensional axial-dispersion model. The mathematical model for the deposition mechanism of asphaltene is written as the material balance of the asphaltene particles in the transient state over a control volume of the pipeline or wellbore.

TABLE 6.1
Capabilities and Limitations of Wellbore Asphaltene Deposition Models

Model	Capabilities	Limitations	Parameters
Vargas et al. (2010)	• Submodels describing particle precipitation, aggregation, transport, and deposition • Two-dimensional convection-diffusion equation • Precipitation modeled using PC-SAFT EoS • Supported by capillary-deposition tests	Aggregation and deposition phenomena modeled using first-order reactions	3
Eskin et al. (2011)	• Submodels describing particle-size distribution evolution in time using PBM and particle transport to the wall using particle-flux mass transfer • Supported by experimental data from RealView	• Experiments on RealView are expensive • Few experimental data are available for tuning parameters	6
Kurup et al. (2012)	• Continuation of the deposition simulator developed by Vargas et al. (2010) • One-dimensional axial dispersion model as it is computationally less expensive • Supported by capillary-deposition tests	• Aggregation mechanism modeled as simple second-order reaction mechanism • One-dimensional model does not capture the entire physics of deposition	3
Vilas Boas Fávero et al. (2016)	• No tuning parameters, but mass transfer coefficient estimated using a correlation • Supported by experimental data from packed-bed column	One-dimensional model does not capture the entire physics of deposition	1
Guan et al. (2017)	• Submodels describing particle precipitation, aggregation, transport, and deposition • Supported by experimental data from capillary-deposition tests • Accounts for the variation in the flow cross-sectional area due to the growing the deposit layer • Uses a fixed mesh	• Transport module is for single-phase flow • Uses PR EoS which is not accurate for asphaltene-precipitation modelling	3

EOS, equation of state; PC-SAFT, perturbed chain statistical associating fluid theory; PBM, population balance model; PR, Peng-Robinson.

6.1.2.1 Assumptions

- Only the asphaltene aggregates, which are smaller than the critical particle size, participate in the deposition process. The large aggregated particles are considered to be carried with the flow because of inertia and do not tend to deposit. In ADEPT, 0.2 μm is assumed as the critical particle size.
- The deposition process is not dominated by transport occurring in the core flow but dominated by transport and kinetics occurring in the laminar boundary layer adjacent to the wall of the wellbore or pipeline. The laminar flow inside a capillary tube mimics the laminar boundary layer occurring in the turbulent wellbore and pipeline flows. Hence, the deposition kinetic constant can be obtained from capillary-deposition experiments.
- The diffusivity of asphaltene particles in the fluid flow is assumed to be constant.

6.1.2.2 Model Development

Step 1: *Precipitation and aggregation kinetics*

The precipitation of asphaltene is modeled as a first-order kinetic process. The kinetics of aggregation is assumed as a second-order kinetic process.

$$\frac{dC'}{dt'} = k_p\left(C'_f - C'_{eq}\right) - k_{ag}C'^2 \tag{6.1}$$

$$\frac{dC'_{ag}}{dt'} = k_{ag}C'^2 \tag{6.2}$$

$$\frac{dC'_f}{dt'} = -k_p\left(C'_f - C'_{eq}\right) \tag{6.3}$$

where:

C' is the dimensional concentration of the primary particles
C'_{ag} is the dimensional concentration of aggregated particles
C'_f is the dimensional concentration of dissolved asphaltene in the oil–precipitant mixture
C'_{eq} is the dimensional thermodynamic equilibrium concentration of asphaltene, which can be regarded as the solubility of asphaltene at the given pressure, temperature, and composition

The value of the precipitation kinetic parameter, k_p, and aggregation kinetic parameter, k_{ag}, can be obtained by solving the Equations 6.1 through 6.3 simultaneously, by minimizing the difference between the experimental data and the modeling results, with the initial condition as the initial molar concentration of asphaltene primary particles solubilized in the oil phase, C_0. The thermodynamic modeling to determine C'_{eq} is performed using the PC-SAFT EoS. The experimental data is obtained by adding a certain amount of precipitant (*n*-heptane) to the oil sample, from which the mass of aggregated asphaltenes can be calculated for different aging times (Kurup et al. 2012), as explained in Section 3.4.

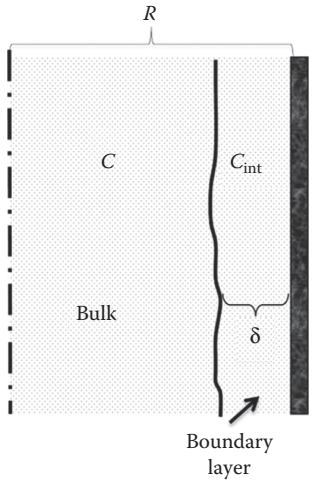

FIGURE 6.1 Laminar boundary near the wall. (Reprinted from Kurup, A. S. et al., *Energy Fuels*, 26, 5702–5710, 2012.)

Step 2: *Mass balance over axial segment of wellbore*

Considering Figure 6.1 and taking into account the assumptions already stated in Section 6.1.2.1, a mass balance can be performed for the axial segment δz as,

$$V_{\text{cell}}\frac{\partial C'}{\partial t'} = -V_{\text{cell}}U_z\frac{\partial C'}{\partial z'} + V_{\text{cell}}D_{ax}\frac{\partial^2 C'}{\partial z'^2} + V_{\text{cell}}k_p\left(C'_f - C'_{eq}\right) - V_{\text{cell}}k_{ag}C'^2 - V_{\text{int}}R_{\text{int}} \quad (6.4)$$

where:

V_{cell} and V_{int} are the volumes of the axial segment and boundary layer segment

R_{int} is the rate of asphaltene depletion because of the deposition process

U_z is the average axial velocity of the fluid

C', C'_f, and C'_{eq} are the dimensional concentration of asphaltene at instant, t', and position, z', dimensional concentration of asphaltene in oil–precipitant mixture and dimensional thermodynamic concentration of asphaltene, respectively

D_{ax} is the axial dispersion coefficient

For laminar flows, such as in the case of capillary-deposition experiments, the dispersion coefficient is calculated using $D_{ax} = D_e + \frac{U_z r^2}{48 D_e}$, provided that the pipe is long enough and the condition that, $D_e\bar{t}\,/\,r^2 > 0.125$ is met. D_e is the particle diffusivity, $\bar{t}$ is the residence time, and r is the radius of wellbore.

Step 3: *Introduction of nondimensional variables*

Introducing nondimensional variables, Equation 6.4 becomes,

$$\frac{\partial C}{\partial t} = -\frac{\partial C}{\partial Z} + \frac{1}{Pe}\frac{\partial^2 C}{\partial Z^2} + Da_p\left(C_f - C_{eq}\right) - Da_{ag}C^2 - \frac{V_{\text{int}}}{V_{\text{cell}}}\frac{L}{U_z}R_{\text{int}} \tag{6.5}$$

where:

$$\frac{V_{\text{int}}}{V_{\text{cell}}} = \frac{2\pi R\delta\Delta Z}{\pi R^2\Delta Z} = \frac{2\delta}{r} \text{ and } R_{\text{int}} = k_d C_{\text{int}} \tag{6.6}$$

The dimensionless parameters are given as

$$Pe = \frac{U_z L}{D_{ax}}, Da_{ag} = \frac{k_{ag}L}{U_z}, Da_p = \frac{k_p L}{U_z}, C = \frac{C'}{C_0},$$

$$C_f = \frac{C_f{}'}{C_0}, C_{eq} = \frac{C_{eq}{}'}{C_0}, Z = \frac{z}{L}, t = \frac{t'U_z}{L}$$

where:

L is the axial length of the wellbore

δ is the boundary layer thickness

Pe, Da_{ag} and Da_p are the non-dimensional numbers, which are defined as follows:

- Peclet number $\left(Pe = \frac{U_z L}{D_{ax}}\right)$ is the ratio of the convective transport rate to that of the diffusive transport rate.
- Precipitation Damköhler number $\left(Da_p = \frac{k_p L}{U_z}\right)$ is the ratio of the precipitation rate to that of the convective transport rate.
- Aggregation Damköhler number $\left(Da_{ag} = \frac{k_{ag}L}{U_z}\right)$ is the ratio of the aggregation rate to that of the convective transport rate.

Step 4: *Rate of asphaltene deposition*

Two competing processes occur in the boundary layer, namely, transport of asphaltene particles into the boundary layer and depletion of asphaltene because of deposition kinetics. At steady-state,

$$R_{\text{mass}.tr} = R_{\text{int}} \tag{6.7}$$

$$\frac{D_e}{\delta^2}\left(C - C_{\text{int}}\right) = k_d C_{\text{int}} \tag{6.8}$$

$$\text{If } \frac{C_{\text{int}}}{C - C_{\text{int}}} = \frac{D_e}{\delta^2 k_d} = \phi, \text{then } C_{\text{int}} = \frac{\phi}{\phi + 1}C \tag{6.9}$$

where:

C is the dimensionless concentration of asphaltene in the bulk

C_{int} is the dimensionless concentration in the boundary layer

k_d is the deposition kinetic constant

The diffusion coefficient is calculated using the Stokes–Einstein relation. Substituting the expression for R_{int} in Equation 6.5, gives the mass balance for the deposition of asphaltene in wellbore,

$$\frac{\partial C}{\partial t} = -\frac{\partial C}{\partial Z} + \frac{1}{Pe}\frac{\partial^2 C}{\partial Z^2} + Da_p\left(C_f - C_{eq}\right) - Da_{ag}C^2 - \frac{V_{\text{int}}}{V_{\text{cell}}}\frac{L}{U_z}k_d C_{\text{int}} \qquad (6.10)$$

Step 5: *Introduction of Scaling Factor*

The mass balance for the deposition of asphaltene in wellbore is given as,

$$\frac{\partial C}{\partial t} = -\frac{\partial C}{\partial Z} + \frac{1}{Pe}\frac{\partial^2 C}{\partial Z^2} + Da_p\left(C_f - C_{eq}\right) - Da_{ag}C^2 - \frac{L}{U_z}k_d^* C \qquad (6.11)$$

$$k_d^* = (k_d)_{\text{cap}}\frac{2\delta}{r}\frac{\phi}{\phi+1} = (k_d)_{\text{cap}}ScF \qquad (6.12)$$

$$ScF = \frac{2\delta}{r}\frac{\phi}{\phi+1} \qquad (6.13)$$

where *ScF* is the scaling factor used to scale the deposition kinetic constant measured using capillary-deposition experiments to that of asphaltene deposition in the wellbore or pipeline.

Step 6: *Initial and boundary conditions*

The required initial and boundary conditions are:

$$C\left(t=0, Z\right) = 0$$

$$C\left(t, Z=0\right) = 0$$

$$\frac{\partial C}{\partial Z}\left(Z=1\right) = 0 \qquad (6.14)$$

AQ 1

Step 5: *Experimental results from capillary deposition test*

To illustrate the application of ADEPT, a capillary-deposition test performed by Kurup et al. (2012) is considered here. The asphaltene-deposition study was conducted in a capillary tube with crude oil (stock-tank oil) and propane (precipitant). The deposition test was performed at 70°C, with a flow rate of 12 cm^3/hr of and oil–propane mixture (Kurup et al. 2012). The asphaltene-deposition profile along the axial length of the capillary tube obtained from the test is shown in Figure 6.2. The deposition-thickness profile shows that the magnitude of asphaltene deposition reaches a maximum at the entrance of the tube because at this point, the driving force for precipitation is maximum. The deposition decreases along the axial

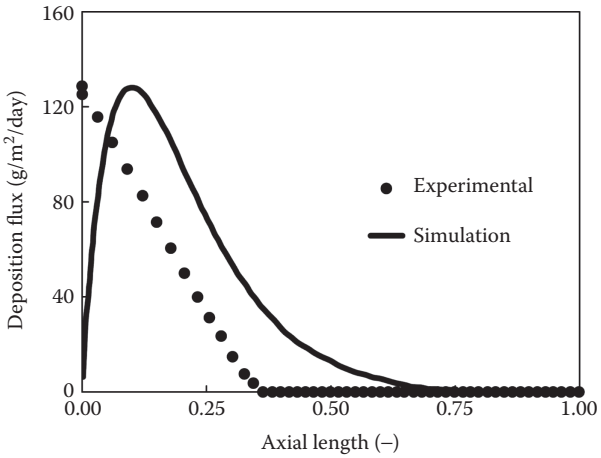

FIGURE 6.2 Comparison of experimental and simulation results for asphaltene-deposition flux along the dimensionless axial length of capillary pipe. (Reprinted from Kurup, A. S. et al., *Energy Fuels*, 26, 5702–5710, 2012.)

length of the tube as the amount of primary particles in the flowing mixture decreases.

Step 6: *Deposition simulator predictions*

In this example, the values of the precipitation and aggregation kinetic parameters were obtained by solving the equations as given in *Step 1*, to find $k_p = 1.32 \times 10^{-3}\ s^{-1}$ and $k_{ag} = 7.29 \times 10^{-3}\ m^3\ mol^{-1}\ s^{-1}$. The deposition-kinetic parameter value is obtained by matching the peak of the deposition-flux profile obtained from experimental data to that of the simulator predictions ($(k_d)_{cap} = 1.4 \times 10^{-3}\ s^{-1}$). The asphaltene-deposition flux along the axial length of the capillary tube obtained from the both the deposition test and ADEPT simulation are shown in Figure 6.2.

The comparison between the two curves shown in Figure 6.2 indicates that the simulation results show a delayed deposition compared to the corresponding experiments. This is because of the simulator being modeled in such a way that asphaltene precipitation begins only at the entrance of the pipe. This means that there is no delay between mixing of oil with the precipitant and entrance of this mixture into the pipe. Choosing a higher value of the deposition constant can decrease this discrepancy; however, this can cause an over-prediction of the deposition-flux peak magnitude compared to experimental measurements

With the simulation of asphaltene deposition in a capillary tube being performed, asphaltene deposition in a wellbore can be predicted now. $(k_d)_{cap}$ value obtained in *Step 6* can be scaled to k_d^* with the help of the scaling factor *ScF*, introduced in Equation 6.13. One such case study is discussed in detail in Section 8.2.1. AQ 2

6.1.3 Modeling Asphaltene Aggregation

Instead of using a simple-reaction mechanism to model an asphaltene-aggregation process (as seen in ADEPT in Section 6.1.2), a population balance model (PBM) can be implemented. Such a model helps to understand the physics of the process more clearly and obtain a particle-size distribution of the asphaltene primary units and aggregates with progress in time. Maqbool et al. (2011) developed a generalized geometric PBM for simulating the growth of asphaltene aggregates from the nanometer scale to micrometer-sized particles. The modeling was performed with respect to results obtained from experiments, where samples were withdrawn from the well-stirred crude oil–heptane mixture at different times and centrifuged. The asphaltene cake obtained as a result of centrifugation was then washed with heptane several times to remove any residual crude oil in the cake, dried in an oven, and weighed to determine the mass of the precipitated asphaltenes (Maqbool et al. 2011). The generation and depletion schemes of the *i*th aggregate were described by four mechanisms, which are shown in Table 6.2.

In Table 6.2, $\bar{R}$ is the geometric spacing between two aggregates and the kinetic parameter, $K_{i,j}$, which is the collision kernel, and is given as $K_{i,j} = \alpha_{i,j}\beta$, where β is the efficiency of collision and $\alpha_{i,j}$ is the collision frequency, which can be represented using the Brownian aggregation kernel as,

$$\alpha_{i,j} = \frac{2RT\left(d_i + d_j\right)^2}{3\mu d_i d_j} \tag{6.15}$$

TABLE 6.2
Mechanism for the Generation and Depletion of the *i*th Aggregate in the Geometric PBE Model

Mechanism	Reaction	Rate of Reaction
Generation 1	$\bar{R}A_{i-1} \rightarrow A_i$	$\left(\frac{dC_i}{dt}\right)_{GM1} = -\frac{K_{i-1,i-1}}{\bar{R}} C_{i-1}^2$
Generation 2	$A_{i-1} + mA_j \rightarrow A_i, j < i-1,$ $m = \left(\bar{R}^{i-1} - \bar{R}^{i-2}\right)/\bar{R}^{j-1}$	$\left(\frac{dC_i}{dt}\right)_{GM2} = C_{i-1}\sum_{j=1}^{i-2} K_{i-1,j}\frac{\bar{R}^{j-1}}{\bar{R}^{i-1} - \bar{R}^{i-2}} C_j$
Depletion 1	$A_i + mA_j \rightarrow A_{i+1}, j < i, m = \left(\bar{R}^i - \bar{R}^{i-1}\right)/\bar{R}^{j-1}$	$\left(\frac{dC_i}{dt}\right)_{DM1} = -C_i\sum_{j=1}^{i-1} K_{i,j}\frac{\bar{R}^{j-1}}{\bar{R}^i - \bar{R}^{i-1}} C_j$
Depletion 2	$A_i + A_j \rightarrow A_i, j \geq i$	$\left(\frac{dC_i}{dt}\right)_{DM2} = -C_i\sum_{j=1}^{N-1} K_{i,j} C_j$

Source: (Adapted from Maqbool et al. 2011).

PBE, Poisson-Boltzmann equation.

where:

d_i and d_j represent the diameters (m) of colliding aggregates i and j
μ is the viscosity of the medium (kg m^{-1} s^{-1})
R is the universal gas constant (R = 8.314 J K^{-1} kmol^{-1})
T is the absolute temperature (K)
β is the single-fitting parameter in this geometric PBM and can be estimated from experimental data involving the growth of the aggregates

The net rate of generation of the ith aggregate is given as sum of the rates of reaction given in Table 6.2, as

$$\frac{dC_i}{dt} = -\frac{K_{i-1,i-1}}{\bar{R}} C_{i-1}^2 + C_{i-1} \sum_{j=1}^{i-2} K_{i-1,j} \frac{\bar{R}^{j-1}}{\bar{R}^{i-1} - \bar{R}^{i-2}} C_j$$
$$-C_i \sum_{j=1}^{i-1} K_{i,j} \frac{\bar{R}^{j-1}}{\bar{R}^{i} - \bar{R}^{i-1}} C_j - C_i \sum_{j=1}^{N-1} K_{i,j} C_j \tag{6.16}$$

These set of coupled ordinary differential equations need to be solved simultaneously to obtain the molar concentration of the ith aggregate as a function of time, with the initial condition being,

$$C_1(0) = \frac{m_A \varphi_o \rho_o}{M_{w,A} N_{\text{agg}}}$$
$$\text{and} \quad C_i(0) = 0 \qquad \text{for } i > 1 \tag{6.17}$$

where:

m_A (kg kg^{-1}) is the mass fraction of destabilized asphaltene per unit mass of oil resulting from the addition of a specified quantity of heptane
φ_o is the volume fraction of oil in the oil–heptane mixture
ρ_o is the oil density

The total mass of destabilized asphaltene per unit volume of the mixture is $m_A \varphi_o \rho_o$. $M_{w,A}$ is the molecular weight of the asphaltene molecules, and N_{agg} is the number of asphaltene molecules per nanoaggregate ($N_{\text{agg}} \approx 8$). And finally, the evolution of the mass of aggregates separated by centrifugation is given by

$$m_A(t) = \frac{\sum_{i=1}^{N} R^{i-1} M_{w,A} s_i C_i(t)}{w_o} \tag{6.18}$$

where:

$m_A(t)$ is the mass of separated asphaltene per unit mass of oil (kg kg^{-1})
w_o is the mass of oil per unit volume of mixture (kg m^{-3})
s_i is the separation efficiency of the ith aggregate in the centrifuge

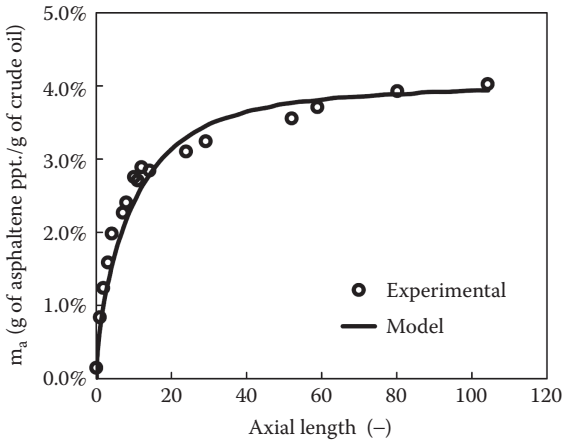

FIGURE 6.3 Experimental and simulated results of the separated aggregates for 50 vol% heptane. (Reprinted from Maqbool, T. et al., *Energy Fuels*, 25, 1585–1596, 2011.)

An example from Maqbool et al. (2011) is illustrated here. The experimental results for the mass of asphaltenes collected by centrifugation at different times for 50 vol% heptane addition to an oil sample and the corresponding simulation results are shown in Figure 6.3.

When this result is combined with the molecular weights for each particle size, a mass-fraction-based particle-size distribution (PSD) can be calculated. The particle-size distribution evolution for 50 vol% heptane addition is shown in Figure 6.4. It should be noted that data markers are the only particle sizes allowed by the geometric PBM, and the connecting lines are only a visual guide.

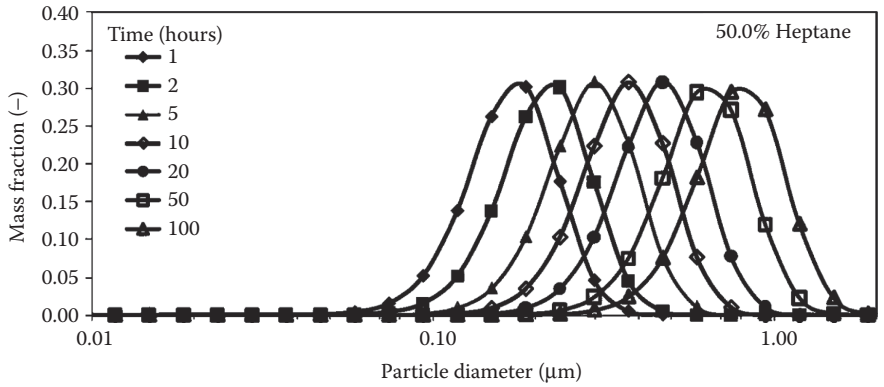

FIGURE 6.4 Particle-size distribution of asphaltene particles as a function of time for 50 vol% heptane with oil. (Reprinted from Maqbool, T. et al., *Energy Fuels*, 25, 1585–1596, 2011.)

6.2 ASPHALTENE DEPOSITION IN POROUS MEDIA

To study and comprehend the deposition tendencies of asphaltenes in porous media, it is important to examine the different ways by which asphaltenes could affect its permeability. Permeability is the property of rocks (porous media), that is, an indication of the ability for fluids (gas or liquid) to flow through the rocks. There are several mechanisms that affect the permeability of porous media. The three most common mechanisms are surface deposition, entrainment, and pore-throat plugging. A new mechanism called *pore-throat opening* was recently introduced (Kord et al. 2014).

- Surface deposition: Asphaltene particles begin to deposit on the surface as a result of gravity or intermolecular forces between asphaltene particles and the surface of the rock (grains). Surface deposition is shown in Figure 6.5a. Here, as crude oil flows into the pore space, asphaltene particles start depositing on the surface (black solid circles).
- Entrainment: When more and more asphaltenes get deposited in the pore, the pore volume becomes smaller, which in turn increases the interstitial velocity and erodes away some of the deposited asphaltenes. The phenomenon of entrainment of the deposited asphaltene is shown in Figure 6.5b (grey solid circles).
- Pore-throat plugging: The pore-throat-plugging mechanism is shown in Figure 6.5c. This mechanism represents the deposition of asphaltene particles in the pore-throat region (black open circles).
- Pore-throat opening: Pore-throat-opening mechanism was proposed by Kord et al. (2014), which is displayed in Figure 6.5d. It is a counterbalance mechanism of pore-throat plugging. When the deposition of asphaltene increases in the pore throat, the cross-sectional area of the pore throat decreases, subsequently increasing the flow rate and thus taking away the deposited asphaltene because of its increased flow rate.

6.2.1 Deposition Models for Porous Media

In the model proposed by Gruesbeck and Collins (1982), three mechanisms (surface deposition, entrainment, and pore plugging) were considered. Two different pathways were considered inside the porous media: pluggable and nonpluggable pathways. Pluggable pathways represented the small pores, which have the potential of to get completely plugged. Nonpluggable pathways denoted the large pores where asphaltene-deposition mechanisms, such as surface deposition and entrainment, take place. As the pore-throat cross-sectional area reduces as a result of asphaltene deposition, the local velocity increases rapidly such that it entrains the deposited asphaltenes out of the pores. Therefore, it was assumed that the large pores could not be totally plugged by the asphaltene aggregates.

Ali and Islam (1998) combined two mechanisms for the simulation of asphaltene deposition in porous media. The first mechanism was the asphaltene adsorption using surface excess theory as examined by Sarwar and Islam (1997), and the other

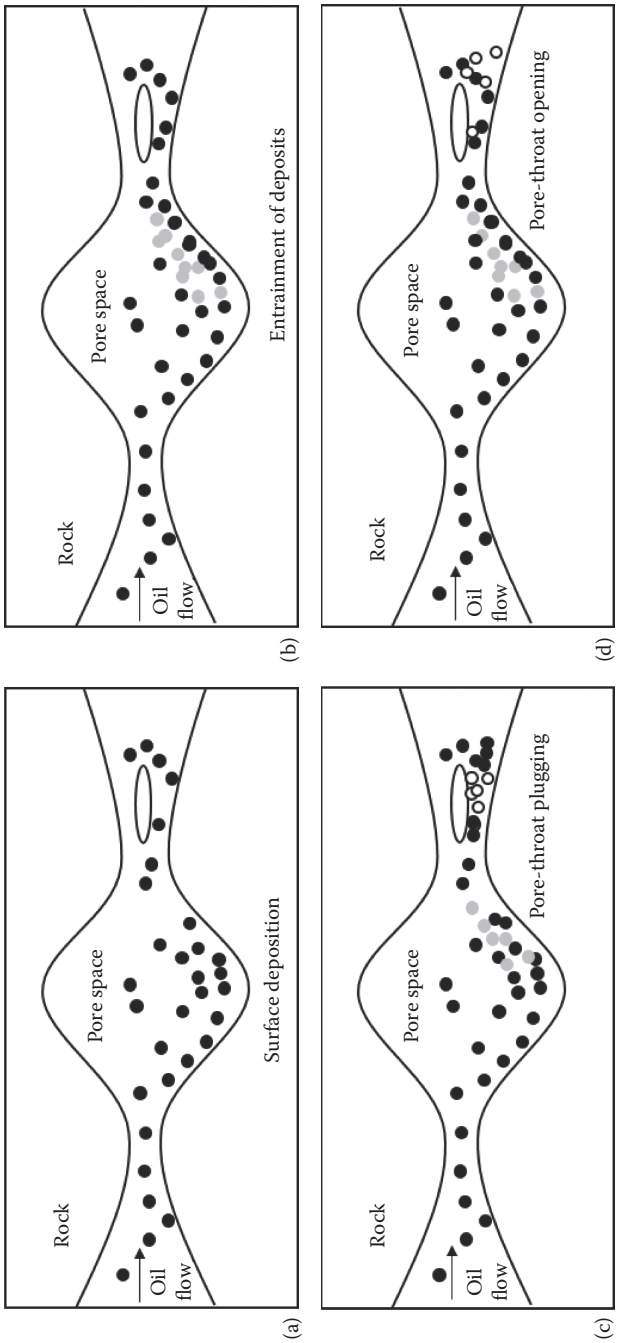

FIGURE 6.5 Mechanisms of deposition: (a) surface deposition, (b) entrainments of deposition, (c) pore-throat plugging, and (d) pore-throat opening. (Reprinted from Kord, S. et al., *Fuel*, 117, 259–268, 2014.)

one was the deposition model proposed by Gruesbeck and Collins (1982). Three different plugging regimes were defined based on the flow rate, namely, monotonous steady-state, quasi–steady-state, and continuous plugging, in the order of lower to higher flow rate (Ali and Islam 1998). In this model, the relationship between porosity and permeability was not considered.

Wang and Civan (2001) modified the Gruesbeck and Collins' (1982) model by considering the relationship between porosity and permeability. A polymer solution theory, developed by Hirschberg et al. (1984) simulating the precipitation process, was combined with the deposition model. This theory along with the mass-balance calculation of the asphaltenes in the required control volume, and porosity and permeability relationship were incorporated into a three-dimensional, three-phase black-oil simulator. The results were verified using the data from core-flooding experiments (Minssieux 1997).

Almehaideb (2004) developed a model to predict precipitation and deposition of asphaltenes in the near-wellbore region, during primary production. For the deposition model, adsorption mechanism, calculated using Langmuir isotherm equation was added to the modified Wang and Civan's (2001) model.

Lawal et al. (2011) investigated the permeability reduction in porous media by applying the deep-bed filtration (DBF) theory along with the kinetics of asphaltene deposition under dynamic conditions. Filtration coefficient, one of the fitting parameters, was used to represent the overall effect because of asphaltene precipitation, flocculation, and deposition. But the model did not include a dispersive term, and the porous media was assumed to be a homogeneous and isotropic system.

Soulgani et al. (2011) developed a model for asphaltene deposition in porous media, where the rate of deposition was predominantly affected by the velocity of the crude oil, the surface temperature, and the asphaltene concentration of the suspension. The deposition model was coupled with a precipitation model (Hirschberg et al. 1984) and the results were verified using the data obtained from core-flooding experiments (Minssieux 1997).

Jafari Behbahani et al. (2015) developed an asphaltene-deposition model that coupled multilayer adsorption and Wang and Civan's model (2001) for mechanical entrapment. The results proved to be in agreement with the experimental data better than the results from Wang and Civan (2001). It was concluded that multilayer kinetic adsorption mechanism plays an important role in asphaltene deposition, wettability alteration, and permeability reduction of the rock.

Kord et al. (2014) modified the surface-deposition mechanism in Wang and Civan (2001) by introducing a new mechanism called *pore-throat opening*. The results from this model matched very well with the core-flooding experimental data.

An analysis of the existing literature reveals that developing an asphaltene-deposition model that can describe deposition mechanisms in porous media accurately including the true physics of deposition is still at initial stages of development. Moreover, all the current models are one-dimensional, and some of these models contain a significant number of fitting parameters; hence, they may have limited applicability and predictive capabilities. Table 6.3 presents the capabilities and limitations of the existing models and lists the number of parameters required

TABLE 6.3
Capabilities and Limitations of Porous Media Asphaltene-Deposition Models

Model	Capabilities	Limitations	Parameters
Gruesbeck and Collins (1982)	• First asphaltene-deposition model • Combination of surface deposition, entrainment, and pore plugging	• Adsorption term neglected • Many fitting parameters • Did not consider the relationship between porosity and permeability	10
Ali and Islam (1998)	Combination of adsorption term and mechanical entrapment	• Too many fitting parameters • Did not consider the relationship between porosity and permeability	16
Wang and Civan (2000)	• Modified Gruesbeck and Collins model • Considered the relationship between porosity and permeability • Fewer fitting parameters • Extendable to field cases	• Neglected adsorption term • Number of fitting parameters slightly high	7
Almehaideb (2004)	Includes adsorption and mechanical entrapment mechanism	Number of fitting parameters slightly high	7
Lawal (2011)	• Considers deep-bed filtration theory • Only three parameters are needed	• Only one parameter is used to represent the effect of asphaltene precipitation, aggregation, and deposition • Can be applied to only homogenous and isotropic system	3
Jafari Behbahanil et al. (2015)	Considered multilayer adsorption	Too many fitting parameters	10
Kord et al. (2014)	• Added pore-throat opening mechanism. • More accurate than Wang and Civan model.	• Number of fitting parameters slightly high • Neglected adsorption term	8

AQ 3

in each case. The Wang and Civan (2001) model is the most popular model used to simulate asphaltene deposition in porous media because it captures most of the asphaltene-deposition mechanisms.

6.2.2 Introduction to Lattice Boltzmann Modeling

The methods adopted for modeling fluid flow can be classified into three main categories: macroscopic, mesoscopic, and microscopic. In macroscopic-scale modeling, fluid is assumed as a continuous medium. The motion of fluid satisfies the

conservation of mass, momentum, and energy. To analyze the fluid flow, nonlinear partial differential Euler equations and Navier-Stokes equations need to be discretized and solved. In microscopic-scale modeling, it is assumed that fluid is composed of many individual molecules. The motion of these molecules is affected by their intermolecular forces and collisions. However, one of the disadvantages of modeling fluid flow based on the microscopic approach includes its excessive computational cost and its inherent limitation to be extended to large-scale systems. Besides macroscopic- and microscopic-flow simulation methods, there is yet another method and is based on mesoscale. In mesoscale modeling, we consider fluid to be a collection of a large number of molecules, instead of focusing on individual molecules as in microscopic approach. Lattice Boltzmann modeling (LBM) method is a mesoscale numerical method.

LBM was first introduced by McNamara and Zanetti (1988). Different from the traditional CFD calculations, LBM is based on molecular kinetic theory. It uses a distribution function to represent the behavior of a group of particles, and thus, saving a large amount of computational memory when compared to the molecular-dynamic simulation techniques (Mohamad 2011; Guo 2013). Moreover, LBM is comparatively easier to implement and more suitable for parallel computing when compared to other traditional CFD discretization methods such as finite difference, finite element, and finite volume methods. LBM can also be readily implemented on complex geometries, which is important for modeling fluid flow in porous media.

There are various equations and parameters that comprise the development of the LBM method, which are introduced in Sections 6.2.2.1 through 6.2.2.4. Before the application of LBM for the prediction of asphaltene deposition in porous media, it is of utmost importance to fathom each of these steps carefully.

6.2.2.1 Distribution Function

To account for a large number of molecules introduced in the LBM, a distribution function was proposed to represent the average effect caused by these molecules. The main idea behind this conceptualization is that the velocity and position of each molecule at any instant of time is not important; instead, the distribution function that represents the corresponding property of the collection of particles is important. The distribution function is given as,

$$f(c) = 4\pi\left(\frac{m}{2\pi k_b T}\right)^{\frac{3}{2}} c^2 e^{-\frac{mc^2}{2k_b T}} \tag{6.19}$$

where:

f is the distribution function
m is the mass of the particle
c is the velocity vector of the particle
T is the temperature
k_b is the Boltzmann constant

6.2.2.2 Boltzmann Transport Equation

The distribution function is then used in a Boltzmann transport equation. Equation 6.20 represents the Boltzmann transport equation.

$$\frac{\partial f}{\partial t} + \frac{\partial f}{\partial \overline{r}} \cdot c + \frac{F}{m} \cdot \frac{\partial f}{\partial c} = \Omega \tag{6.20}$$

where:

F represents an external force
$\overline{r}$ is the position vector of the particle
Ω is the collision operator

6.2.2.3 The BGK Model

To overcome the problem of complexity of the collision term in the Boltzmann equation, Bhatnagar, Gross, and Krook (BGK; 1954) used a simplified model to represent the collision operator, which is given as,

$$\Omega = \sigma\left(f^{eq} - f\right) = \frac{1}{\tau}\left(f^{eq} - f\right) \tag{6.21}$$

where:

σ is the collision frequency
τ is the relaxation factor
f^{eq} is the local equilibrium distribution function

Substituting the BGK approximation in the Boltzmann equation,

$$\frac{\partial f_i}{\partial t} + c_i \nabla f_i = \frac{1}{\tau}\left(f_i^{eq} - f_i\right) \tag{6.22}$$

which is the LBM discretized Boltzmann equation. This equation is only valid along some specific directions. To decide the specific directions in which the particles should move, a lattice arrangement is required in LBM.

6.2.2.4 Lattice Arrangement

In LBM, the most common way to represent the lattice arrangement is using the DnQm notation, where *n* refers to the number of dimensions and *m* refers to the number of directions that the particles can move. Here are some examples of lattice arrangement normally used in LBM.

- One-dimensional: The most common lattice arrangement for one-dimensional LBM is D1Q2 and D1Q3, which are shown in Figure 6.6a. In D1Q2 arrangement, particles can move to the right or left, whereas, in D1Q3 arrangement, in addition to moving left or right, particles have one more choice to stay at their original position.

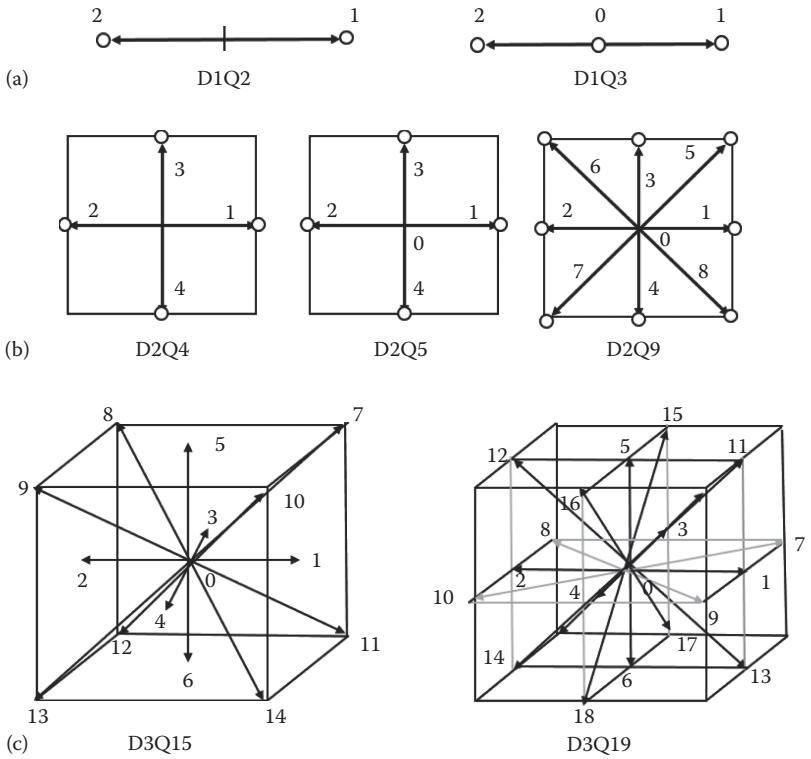

FIGURE 6.6 Lattice arrangements for (a) one-dimensional, (b) two-dimensional, and (c) three-dimensional lattice Boltzmann method. (a and b, Adapted from Guo, Y. and M. Wang, M., *J. Comput. Phys.*, 315, 1–15, 2016; c, Reprinted from Delbosc, N. et al., *Comput. Math. Appl.*, 67, 462–475, 2014.)

- Two-dimensional: The lattice arrangement for two-dimensional LBM are D2Q4, D2Q5, and D2Q9 as shown in Figure 6.6b. In D2Q4, the particles can move in four directions and in D2Q5, additionally, the particles can stay at their original position. In D2Q9 arrangement, particles can move in eight directions or stay at their original position.
- Three-dimensional: There are two kinds of lattice arrangement for three-dimensional LBM, namely, D3Q15 and D3Q19, which are shown in Figure 6.6c. D3Q15 is the most common arrangement used for three-dimensional modeling. (Nit et al. 2013; Premnath et al. 2013). More details on LBM and the implementation of LBM can be found in Mohamad (2011).

6.2.3 Application of LBM

LBM has proved to be an effective method to simulate flow in porous media. Succi et al. (1989) first applied LBM to calculate the three-dimensional flow in a porous medium. The relationship between porosity and permeability was also established.

Heijs and Lowe (1995) applied LBM to study the permeability reduction using Carman-Kozeny equation (Carman 1939) for porous media composed of a random array of spheres and also for clay soil. Ferréol and Rothman (1995) used three-dimensional tomographic skill to reconstruct the Fontainebleau sandstone. The accuracy of LBM simulation was better for samples of larger size. Simulation results agreed well with the data from laboratory experiments. Hence, LBM can now be used to model asphaltene deposition in porous media as well.

As described in Section 5.1.2.2, asphaltene deposition in porous media is studied at laboratory scale using microfluidic devices (microchannel) and core-flooding experiments. The application of LBM to model asphaltene deposition occurring in a microchannel is illustrated in the following subsections. By incorporating the complexities of channel geometry, fluid-flow rates, diffusion coefficients, and possible chemical interactions into a LBM, the behavior of the particular system can be accurately predicted.

6.2.3.1 Assumptions

- The fluid is assumed to be incompressible and Newtonian in nature with constant viscosity.
- The third dimension, depth of the device, is small compared to the other two dimensions such that a shallow planar configuration is created. The governing equation becomes identical to that of the potential flow (which characterized by an irrotational velocity field) and to the flow of fluid through a porous medium (Darcy's law). It thus permits visualization of this kind of flow in two dimensions.
- The flow is fully developed and laminar.
- The energy dissipation is negligible, and hence, there is no heat transfer to or from the ambient medium.

6.2.3.2 Model Development

Microfluidic devices facilitate in the experimental determination of asphaltene deposition in porous media at laboratory scale. Microchannel experiments and their capabilities were discussed in detail in Section 5.1.2.2. In this section, one such experiment performed by He et al. (2017) will be used to illustrate the application of LBM and further simulate asphaltene deposition in the microchannel geometry.

Step 1: *Microchannel geometry*

The microchannel geometry for LBM simulation is built as per the device used by He et al. (2017) for their deposition tests. The experiment was performed at ambient pressure and temperature in a microchannel of length 1.91 mm, width 1.8 mm, and depth 0.02 mm. A number of circular posts of diameter 0.125 mm were present in the device, which in turn acted as an obstacle to the fluid flow and served as a surface for deposition. The porosity of the microchannel was 0.85.

Crude oil and a precipitant (*n*-heptane) were injected into the microchannel. The density and viscosity of the fluid mixture were 0.72 g/cm^3 and 0.5 cP, respectively. The flow rate was maintained at 100 µl/min.

Step 2: *Governing equations for fluid flow*

The continuity equation is given as,

$$\frac{\partial(\rho u)}{\partial x}+\frac{\partial(\rho v)}{\partial y}=0 \tag{6.23}$$

where:

u and v represent the velocity fields in x and y directions, respectively

ρ is the density of the fluid in the microchannel

Momentum transfer in x and y directions is given by the following Navier–Stokes equations:

$$\frac{\partial(\rho u)}{\partial t}+\frac{\partial(\rho uu)}{\partial x}+\frac{\partial(\rho vu)}{\partial y}=-\frac{\partial p}{\partial x}+\frac{\partial}{\partial x}\left(\mu\frac{\partial u}{\partial x}\right)+\frac{\partial}{\partial y}\left(\mu\frac{\partial u}{\partial y}\right) \tag{6.24}$$

$$\frac{\partial(\rho v)}{\partial t}+\frac{\partial(\rho uv)}{\partial x}+\frac{\partial(\rho vv)}{\partial y}=-\frac{\partial p}{\partial y}+\frac{\partial}{\partial x}\left(\mu\frac{\partial v}{\partial x}\right)+\frac{\partial}{\partial y}\left(\mu\frac{\partial v}{\partial y}\right) \tag{6.25}$$

where:

p is the pressure

μ is the viscosity of the fluid

Step 3: *Fluid flow simulation using LBM*

As described in detail in Section 6.2.2, the velocity vector is written in terms of the Boltzmann Equation 6.20, with the collision operator expressed in terms of the BGK model as described in Equation 6.21. Once the BGK model is applied to the Boltzmann equation, a LBM discretized Boltzmann equation is obtained, as shown in Equation 6.22. And as two-dimensional modeling is performed for a microfluidic device, the D2Q9 lattice arrangement is used.

The boundary conditions are applied in such a way that velocity is known at the inlet and pressure (=1 atm) at the outlet. On the wall surfaces and on the surface of the circular posts, no slip boundary condition is applied.

Step 4: *Modeling asphaltene deposition*

Asphaltene deposition is initiated by the addition of the precipitant (*n*-heptane) in the microchannel. The deposition process is modeled using a two-dimensional convection-diffusion-reaction equation.

The mass balance of the suspended asphaltene particles in the required control volume of the microchannel is given as,

$$\frac{\partial m}{\partial t} + \nabla \cdot (\boldsymbol{u}m) = \nabla \cdot \left(D_e \nabla m \right) + R_p - R_{ag} - R_d \tag{6.26}$$

where:

- m and m_D represent the mass fraction of the suspended and deposited asphaltene in the crude oil, respectively
- D_e is the diffusivity of the asphaltenes in the fluid medium
- $\boldsymbol{u}$ is the velocity field, which is obtained by solving the momentum transfer equations using LBM as shown in *Step 3*
- R_p, R_{ag}, and R_d represent the rates of asphaltene precipitation, aggregation, and deposition, respectively

In the present example, the rates R_p and R_{ag} are neglected for simplicity. Nevertheless, the rate of asphaltene precipitation can be explicitly calculated if needed, based on the supersaturation degree, which is the difference between the actual concentration of asphaltene in the oil–precipitant mixture and the concentration of asphaltene at thermodynamic equilibrium as shown in Equation 6.3. PC-SAFT EoS (Section 4.4.2) can be used to calculate the thermodynamic equilibrium concentration of asphaltene at a particular pressure and temperature. The rate of aggregation can also be modeled using a simple reaction mechanism as shown in Equation 6.2. The rate of asphaltene deposition in the microchannel is modeled as,

$$R_d = -\frac{\partial m_D}{\partial t} = a * m * \frac{\partial u}{\partial x} + b * u \tag{6.27}$$

In Equation 6.27, the first term on the right-hand side of the equation demonstrates surface-deposition mechanism and the second term indicates the entrainment mechanism. a and b are the phenomenological constants. a is called the *surface-deposition coefficient*, and b is the entrainment coefficient.

Step 5: *Estimation of deposition-model parameters*

The surface-deposition and entrainment-coefficient values for simulation of asphaltene deposition in the microchannel are obtained by tuning the results from the deposition model against the data obtained from the microfluidic experiments. For this example, the value of a is estimated as 1.69×10^{-5}, and the value of b is 3.69×10^{-3} m^{-1}. The experimental and simulation results for the mass of deposited asphaltene with respect to the injected pore volume are shown in Figure 6.7. The effect of oil–precipitant mixture flow rate on asphaltene deposition, permeability reduction caused thereby in the microchannel, and many more interesting results are discussed for a case study in Section 8.2.3.

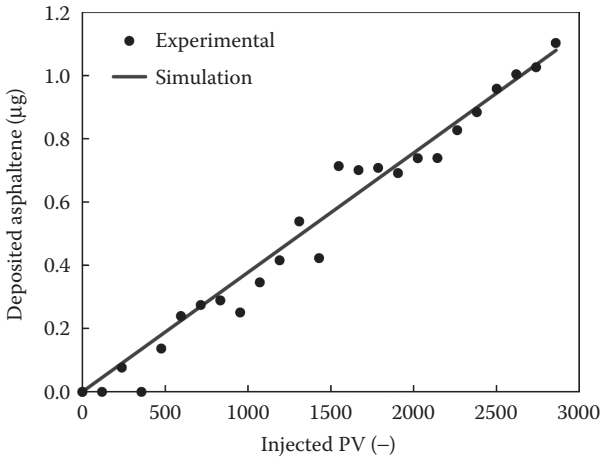

FIGURE 6.7 Amount of deposited asphaltene as a function of injected pore volume for a flow rate 100 μl/min in microchannel. (Experimental results from He et al. 2017.)

6.3 MODELING OF ASPHALTENE-TRANSPORT PROPERTIES

Asphaltene-transport properties are important parameters required in the deposition model. While investigating asphaltene deposition in wellbore, transportation pipelines, or porous media, asphaltene-transport properties, such as density, viscosity, and diffusion coefficient at that particular pressure and temperature conditions need to be clearly specified. In this section, prediction and calculation of density, viscosity, and diffusion coefficient of asphaltenes will be discussed in detail.

6.3.1 Density

Density is often calculated along with phase-behavior calculation using the same EoS, so that thermodynamic description of phase compositions and properties are consistent. Density, ρ, can be expressed as the following,

$$\rho = \frac{M}{V} \tag{6.28}$$

where:
M is the molecular weight
V is the molar volume

When working with mixtures, the mixture average molecular weight, M_{mix}, and mixture molar volume, V_{mix}, are used instead of M and V. M_{mix} can be calculated from the phase composition solved from flash calculation (Section 4.1),

$$M_{\text{mix}} = \sum_{i=1}^{N} x_i M_i \tag{6.29}$$

where x_i is the mole fraction of component i. The molar volume for mixture, V_{mix}, is calculated from the compressibility factor, Z, which is in turn obtained by using an EoS for a given temperature, T, and pressure, P, using Equation 6.30:

$$V_{mix} = \frac{Z \cdot R \cdot T}{P} \tag{6.30}$$

where R is the ideal gas constant.

6.3.2 Viscosity

Viscosity is a transport property necessary to simulate fluid-flow behavior. The viscosity of hydrocarbon fluids can vary by several orders of magnitude not only because of variation in temperature, pressure, and compositions but also because of the presence of aggregated-asphaltene suspension particles when the solution becomes thermodynamically unstable. Therefore, having an accurate viscosity model is important to predict the asphaltene deposition in the wellbore and porous media.

Viscosity models that are applicable to hydrocarbon systems have been thoroughly reviewed (Mehrotra et al. 1996; Vesovic et al. 2014). The gas-phase viscosity can be well predicted by models based on the kinetic theory and Chapman-Enskog theory (Mehrotra et al. 1996). The kinetic theory bridges transport properties to molecular properties for dilute gases, where the Boltzmann Equation is solved using the Chapman-Enskog theory. On the other hand, predicting the liquid-phase viscosity is more challenging. The viscosity models for the liquid phase are usually classified into empirical models and semi-theoretical models. Semi-theoretical models are adopted in industries compared to empirical models because they offer a better performance. The Lohrenz-Bray-Clark (LBC) method, based on the viscosity correlation proposed by Jossi et al. (1962) is an exception, albeit being an empirical model. The LBC method to predict viscosity is often the preferred method in reservoir simulation because of its simplicity and low-computational cost compared to the more accurate semi-theoretical models. Although the method is simple, the LBC method is known to provide results of low quality (Pedersen et al. 2015). Hence, although modeling processes that require greater accuracy, application of semi-theoretical models is recommended. Viscosity models for petroleum fluids specifically are often broadly classified either as black-oil-approach models or compositional models. Compositional models are usually semi-theoretical. Semi-theoretical models often applied in the industry are the corresponding state principle (CSP) and friction theory (f-theory). Although hard-sphere based models such as the Dymond and Assael approach (Assael et al. 1992) and the Vesovic-Wakeham (VW) model (1989) have found some practical applications, a dependable and consistent model to predict viscosity for petroleum fluids is not always readily available.

6.3.2.1 Lohrenz-Bray-Clark (LBC) Method

The LBC method (Lohrenz et al. 1964) adopted the viscosity correlation developed by Jossi et al. (1962) for pure components. The viscosity correlation is a fourth-degree polynomial in reduced density ρ_r, which is expressed as,

$$((\mu - \mu^*)\xi + 10^{-4})^{1/4} = a_1 + a_2\rho_r + a_3{\rho_r}^2 + a_4{\rho_r}^3 + a_5{\rho_r}^4 \tag{6.31}$$

$$\xi = \frac{\left(\sum_{i=1}^{nc} z_i T_{ci}\right)^{1/6}}{\left(\sum_{1}^{nc} z_i M_i\right)^{1/2}\left(\sum_{i=1}^{nc} z_i P_{ci}\right)^{2/3}} \tag{6.32}$$

$$\rho_r = \rho/\rho_c \tag{6.33}$$

$$\rho_c = \frac{1}{V_c} = \frac{1}{\sum_{i=1}^{nc} z_i \hat{V}_{ci}} \tag{6.34}$$

where:

μ is the viscosity
ξ is the viscosity-reducing parameter
a_i represents the viscosity correlation polynomial coefficients
ρ_r is the reduced density
μ^* is the low-pressure gas mixture viscosity
z_i is the mole fraction of component i
ρ_c is the critical density
$\hat{V}_c$ is the critical molar volume

The default values of coefficients a_i are provided in Table 6.4, which were regressed to viscosity data of 11 lighter gases, the heaviest being *n*-pentane (Jossi et al. 1962).

Lohrenz et al. (1964) suggested calculating the critical density of a crude oil as follows,

$$\rho_c = \frac{1}{V_c} = \frac{1}{\sum_{\substack{i=1 \\ i \neq c7+}}^{nc} z_i V_{ci} + z_{C7+} V_{cC7+}} \tag{6.35}$$

TABLE 6.4
Default Values of Coefficients in the Viscosity Correlation in LBC Method

Parameters in LBC Model	Default Values
a_1	0.10230
a_2	0.023364
a_3	0.058533
a_4	−0.040758
a_5	0.0093324

LBC, Lohrenz-Bray-Clark.

where *nc* refers to the number of components, and the critical molar volume of the C7+ fraction V_{cC7+} can be estimated from,

$$V_{cC7+} = 21.573 + 0.015122M_{C7+} - 27.656G_{C7+} + 0.070615M_{C7+} \cdot G_{C7+} \tag{6.36}$$

Based on the C7+ fraction molecular weight M_{C7+} and specific gravity G_{C7+}.

The V_C of pseudo-components and the five coefficients a_i can be treated as tuning parameters in the LBC method to obtain better modeling accuracy. The parameter tuning must be undertaken with extreme caution to avoid nonphysical predictions from the fourth-degree polynomial formulation. Because of this concern and the limited viscosity data collected from routine pressure, volume, and temperature experiments, parameter tuning for LBC method can be challenging in the practice.

6.3.2.2 Friction Theory

Since Quiñones-Cisneros et al. (2000) proposed the friction theory, it has been applied to model viscosity for a wide range of fluids including alkanes, natural gas, crude oil, heavy oil, and blends (Quiñones-Cisneros et al. 2000, 2001, 2005; Zeberg-Mikkelsen et al. 2002; Schmidt et al. 2005; Abutaqiya et al. 2017). Friction theory conceptualizes viscosity as a mechanical property instead of a transport property. Viscosity is expressed as a sum of two viscosity contributions,

$$\mu = \mu_0 + \mu_f \tag{6.37}$$

where:

μ_0 represents the dilute gas contribution
μ_f represents the friction contribution

The dilute gas contribution, μ_0, can be determined from the model based on the Chapman-Enskog theory (Chung et al. 1988; Quiñones-Cisneros et al. 2001). Quiñones-Cisneros et al. (2000) correlated the friction contribution to the repulsive and attractive pressure terms by analogy with the Amontons-Coulomb friction law (Quiñones-Cisneros et al. 2000). For a cubic EoS, the friction contribution is formulated as follows,

$$\frac{\mu_f}{\mu_c} = \hat{\mu}_f = \hat{k}_a P_a + \hat{k}_r P_r + \hat{k}_{rr} P_r^2 \tag{6.38}$$

where:

μ_c is the characteristic critical viscosity
$\hat{\mu}_f$ is the dimensionless friction viscosity contribution
$\hat{k}$ is the viscosity friction coefficient
The subscript *r*, *a*, and *rr* represent repulsive, attractive, and second-order repulsive term, respectively
P_r and P_a are the repulsive and attractive pressures that can be obtained from a typical cubic EoS

For the Peng-Robinson EoS, P_a and P_r are calculated from the following expression,

$$P_a = -\frac{a}{\hat{V}^2 + 2\hat{V} \cdot b - b^2} \tag{6.39}$$

$$P_r = \frac{R \cdot T}{\hat{V} - b} \tag{6.40}$$

where the same nomenclature is used as PR EoS which was introduced in Section 4.2.3.1. The characteristic critical viscosity, μ_c, of light alkanes can be found in Quiñones-Cisneros et al (2001). For undefined components, the characteristic critical viscosity, η_c, can be estimated from a correlation (Uyehara and Watson 1944),

$$\mu_{c,i} = K_c \frac{M_i^{1/2} P_{c_i}^{2/3}}{T_{c_i}^{1/6}} \tag{6.41}$$

where K_c is the critical viscosity constant, typically tuned against available viscosity data. The expressions and constants to calculate viscous friction coefficients $\hat{k}_a$, $\hat{k}_r$, and $\hat{k}_{rr}$ can be found in Quiñones-Cisneros et al. (2001).

Abutaqiya et al. (2017) have modeled the live oil viscosity of 10 different crudes using the Peng-Robinson EoS version of the friction theory (PR-FT) as seen in Figure 6.8 (Abutaqiya et al., in preparation). The properties of the crude oils modeled are listed in Table 6.5. The characterization procedure used is the saturate, aromatic, resin, and asphaltene (SARA)-based method, which has been discussed in Section 4.3.1. The general procedure for applying friction theory for modeling live oil viscosity is, AQ 5

1. Characterize crude oil based on the compositional analysis and phase-behavior information provided in the PVT report (discussed in Section 4.3)
2. Create pseudo-components and their EoS parameters that predict the correct phase behavior (also discussed in Section 4.3)
3. Tune the critical viscosity constant, K_c, in Equation 6.41 to match the available viscosity data.

Abutaqiya et al. (2017) obtained an overall average absolute percent deviation (AAPD) of 3.7% for the live oil viscosity modeling using the SARA-based characterization and Peng-Robinson EoS version of the friction theory by tuning K_c to viscosity data at saturation point. The average absolute percent deviation for predictions above P^{sat} was 1.8% overall.

6.3.2.3 Corresponding State Principle Models

The corresponding state principle (CSP) has been widely used to model properties of substances (Ely and Hanley 1981; Pedersen et al. 1984). The CSP model for viscosity prediction proposed by Pedersen et al. (1984) was developed from the work of Ely and Hanley (1981) and has found industrial application as well.

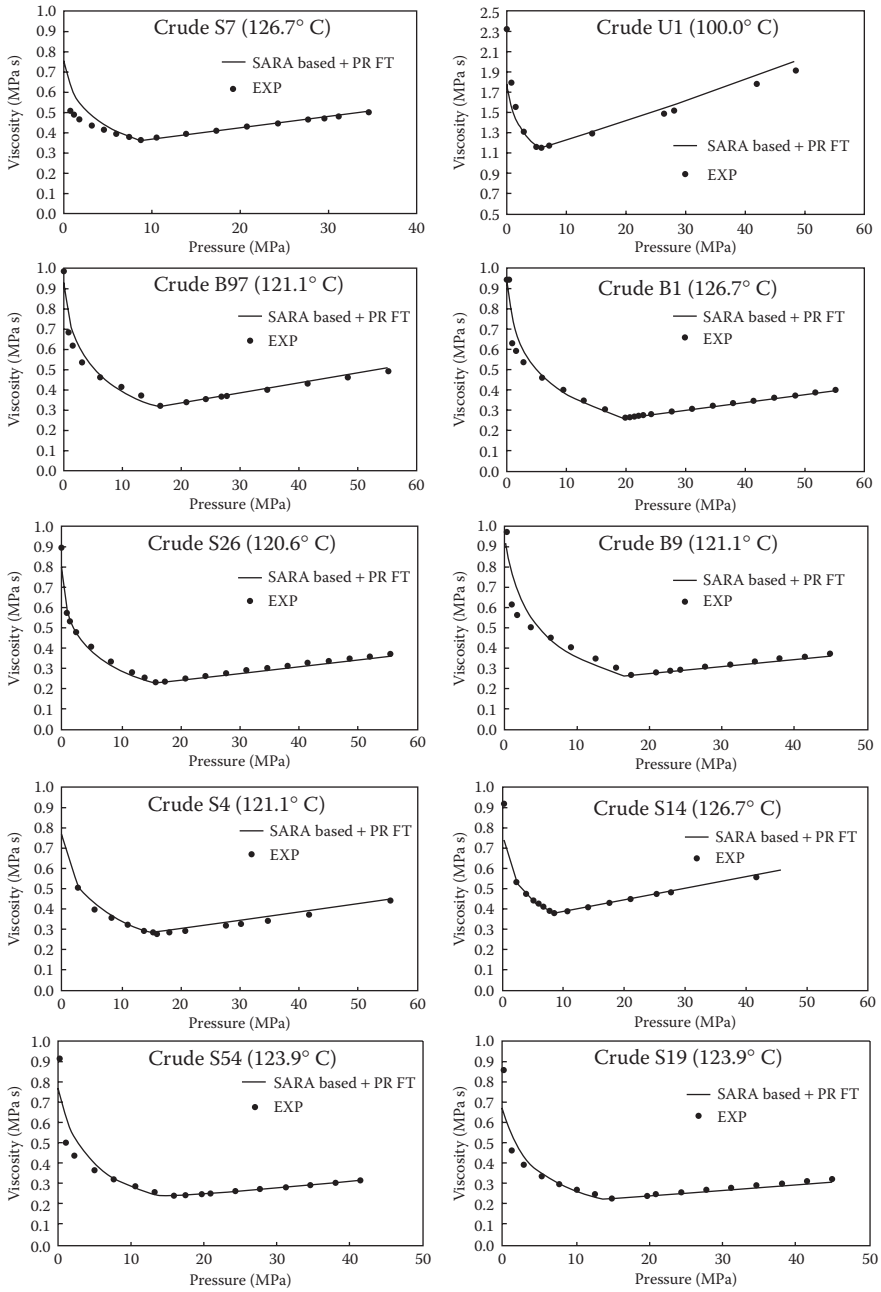

FIGURE 6.8 Live-oil viscosity-modeling results using SARA-based characterization and Peng-Robinson friction theory. SARA, saturates, aromatic, resin, and asphaltene. (Reprinted from Abutaqiya et al. 2017)

TABLE 6.5
Properties of Crude Oils Modeled

Property \ Crude	S7	U1	B97	B1	S26	B9	S4	S14	S54	S19
STO MW (g/mol)	201.5	212.4	201.9	204.0	193.5	208.0	177.5	181.2	193.0	189.7
STO API gravity	37.4	31.7	36.9	36.9	40.5	38.0	40.2	39.2	38.4	39.7
GOR (Sm^3/m^3)	83.5	38.1	147.8	192.4	189.7	163.7	135.4	63.4	171.4	159.1
ρ^{sat} (kg/m^3)	692.0	764.0	654.7	636.2	624.2	647.6	643.0	692.0	632.4	635.5
Reservoir temperature (°C)	126.7	100.0	121.1	126.7	120.6	121.1	121.1	126.7	123.9	123.9
P^{sat} (MPa)	8.79	5.76	16.39	19.79	15.79	17.35	15.41	7.63	15.88	14.81
Saturates, wt%	68.6	59.4	70.42	70.2	49.5	—	68.9	68.6	—	—
Aromatics, wt%	22.3	22.57	22.64	22.9	40.2	—	21.8	22.3	—	—
Resins, wt%	6.6	13.97	6.24	4.9	7.2	—	7.1	6.5	—	—
Asphaltene wt%	0.4	1.73	0.18	0.1	3.1	—	0.5	0.5	—	—

Source: Abutaqiya et al., (2017).
GOR, gas-to-oil ratio; MW, molecular weight; STO, stock-tank oil.

Ely and Henley expressed reduced viscosity, μ_r, for substances that are members of a homologous series as,

$$\mu_r(\rho, T) = \frac{\mu(\rho, T)}{T_c^{-1/6} P_c^{2/3} M^{1/2}} \tag{6.42}$$

where:
- ρ is the density
- T is the temperature
- T_c is the critical temperature
- P_c is the critical pressure
- M is the molar mass

The model by Pedersen et al. (1984) uses variables T and P instead of T and ρ as in Ely and Hanley's model (Tham and Gubbins 1970). For a crude-oil mixture, Pedersen et al. proposed the viscosity of mixture μ_{mix} at a given T and P as,

$$\mu_{\text{mix}} = \left(\frac{T_{c,\text{mix}}}{T_{co}}\right)^{-1/6} \left(\frac{P_{c,\text{mix}}}{P_{co}}\right)^{2/3} \left(\frac{M_{\text{mix}}}{M_o}\right)^{1/2} \left(\frac{\alpha_{\text{mix}}}{\alpha_o}\right) \eta_o\left(P_o, T_o\right) \tag{6.43}$$

$$P_o = \frac{P P_{co} \alpha_o}{P_{c,\text{mix}} \alpha_{\text{mix}}} \tag{6.44}$$

$$T_o = \frac{T T_{co} \alpha_o}{T_{c,\text{mix}} \alpha_{\text{mix}}} \tag{6.45}$$

$$\alpha_{\text{mix}} = 1 + 7.378 * 10^{-3} \rho_r^{1.847} M_{\text{mix}}^{0.5173} \tag{6.46}$$

where:
- The subscript mix represents the hydrocarbon mixture
- The subscript o represents the reference state
- α is the rotational coupling coefficient

Pedersen et al. (1984) included the rotational coupling coefficient (α) suggested by Tham and Gubbins to the viscosity CSP model to correct for the deviation from the simple CSP behavior. α can be treated as an adjustable parameter. Pedersen et al. (1984) improved the viscosity prediction by adopting the mixing rule to calculate the mixture molecular weight, M_{mix}

$$M_{\text{mix}} = \overline{M_n} + 1.304 \times 10^{-4} \left(\overline{M_w}^{2.303} - \overline{M_n}^{2.303}\right) \tag{6.47}$$

$$\overline{M_w} = \frac{\sum_{i=1}^{nc} z_i M_i^2}{P_{ci}} \tag{6.48}$$

$$\overline{M_n} = \sum_{i=1}^{N} z_i M_i \tag{6.49}$$

6.3.2.4 Effect of Asphaltene Precipitation on Apparent Viscosity of Oil

Asphaltene precipitation is known to increase the apparent viscosity and cause complex viscosity behavior (Barré et al. 2008; Eyssautier et al. 2012; Chávez-Miyauchi et al. 2013; Tavakkoli et al. 2013; Hashmi et al. 2015). Chávez-Miyauchi et al. (2013) summarized from several studies that asphaltene suspension behaves as a dilute system at asphaltene concentration below 10 wt%, and the suspension behaves as a concentrated system at asphaltene concentration above 10 wt%. Properties of the precipitated asphaltenes, such as rate of aggregation, aggregate size distribution, and concentration affect the apparent crude-oil viscosity. The viscosity behavior of a dilute suspension of rigid spheres can be modeled using the Einstein equation as,

$$\mu_r = 1 + [\mu]\phi \tag{6.50}$$

where relative viscosity, μ_r, is expressed as a function of the intrinsic viscosity, $[\mu]$, and the volume fraction of suspended particles, ϕ. To account for the deviation from the ideal behavior predicted using the Einstein equation, researchers have extended the model to reflect the effect of higher particle concentrations, solvation, and nonsphericity (Mooney 1951; Krieger and Dougherty 1959; Pal and Rhodes 1989). The viscosity models for suspensions proposed by Kreger and Dougherty and that by Pal and Rhodes (1989) have been frequently used to interpret and model asphaltene suspension behaviors. Krieger and Dougherty proposed that the relative viscosity, μ_r, for a suspension can be modeled according to Equation 6.51.

$$\mu_r = \left(1 - \frac{\phi}{\phi_m}\right)^{-[\mu]\phi_m} \tag{6.51}$$

where:

ϕ is the volume fraction of the suspended particles
ϕ_m is the maximum packing volume fraction
$[\mu]$ is the intrinsic viscosity

Pal and Rhodes (1989) suggested that the relative viscosity of a Newtonian emulsion can be expressed as

$$\mu_r = \left(1 - K_0\phi\right)^{-2.5} \tag{6.52}$$

where K_0 is the *solvation* coefficient. K_0 is intended to correct for the increased effective volume fraction because of the immobilized continuous phase at the surface of the dispersed particles. It was concluded that the Pal and Rhodes (1989) model is unsuitable for modeling asphaltene suspensions because the derivation assumed modeling a suspension of spherical particles and the effect of maximum packing of

particles was not considered (Pal and Vargas 2014). Pal and Vargas (2014) reinterpreted 14 sets of viscosity measurements for asphaltene suspensions in various liquid media using the Krieger and Dougherty model. It was found that the maximum packing-volume fraction of particles was nearly constant across all data available regardless of their temperature and the nature of asphaltene systems. Hence, Pal and Vargas (2014) proposed that asphaltene suspension can be modeled with the Krieger and Dougherty model, as,

$$\mu_r = \left(1 - \left(\frac{\phi}{0.37}\right)\right)^{-0.37[\eta]} \tag{6.53}$$

With the maximum packing volume fraction $\phi_m = 0.37$.

6.3.3 Diffusion Coefficient

A review of the asphaltene-deposition models developed over the years shows that the calculation preformed to estimate the value of diffusion coefficient, used either in a convection-diffusion transport equation or population balance equations, has been highly influenced by the experimental technique adopted, operating conditions, and properties of the precipitant used to initiate deposition.

In the deposition simulator developed by Vargas et al. (2010), the diffusion coefficient of 0.35×10^{-9} m^2/s for asphaltenes in toluene is assumed as a rough approximation for its diffusivity in the oil–precipitant mixture used in the capillary-deposition test. This value was obtained using fluorescence correlation spectroscopy (FCS) at extremely low concentrations (0.03–3.0 mg/l), where aggregation does not occur corresponding to a hydrodynamic radius of approximately 1 nm (Andrews et al. 2006).

In ADEPT (developed by Kurup et al. 2012), the diffusion coefficient was calculated using the Stokes–Einstein relation, which is given as,

$$D_e = \frac{k_b T}{6\pi \nu_f r_{cr}} \tag{6.54}$$

where:

k_b is the Boltzmann constant
T is the temperature of the fluid
ν_f is the kinematic viscosity of the fluid
r_{cr} is the critical size of asphaltene particles in the oil–precipitant mixture

While modeling asphaltene deposition based on experiments carried out in RealView, a cylindrical Couette-Taylor system, asphaltene gets deposited on the outer stationary wall as the inner cylinder rotates at very high speeds (Section 5.1.1.3). For turbulent flows, the eddy diffusion as a result of the fluctuating velocity components and the consequent turbophoresis governs the deposition of aggregated asphaltene on the outer cylinder wall surface. Thus, the particle diffusivity, D_p, in a turbulent flow can be calculated as: $D_p = D_t + D_B$, where D_t is the turbulent particle diffusivity and

D_B is the Brownian diffusivity. Because the particles are small (as critical particle size is of the order of nanometers), the particle diffusivity is approximately equal to the eddy diffusivity ($D_p = D_t$), as the Brownian diffusivity plays a significant role for submicron particles only (Eskin et al. 2011). For the sake of convenience, the particle-deposition flux only at the laminar-boundary-sublayer surface can be considered, where the deposition of the asphaltenes to the cylinder surface takes place. The eddy diffusivity at the laminar-sublayer surface is given as, $D_t = \nu_t/Sc_t$, where ν_t is the eddy diffusivity (m^2/s) and Sc_t is the turbulent Schmidt number. Hence, essentially the calculation of the diffusion coefficient is dependent on the properties of the fluid and flow regimes of the asphaltene-deposition experimental techniques.

6.4 FINAL REMARKS

Several significant advancements have been made in developing tools for the investigation and modeling of asphaltene deposition in the wellbore during oil production operations. A detailed review of the modeling of asphaltene deposition in both wellbore and porous media, developed over the years has been has been presented. The development of ADEPT to predict asphaltene deposition in wellbore and pipelines has been discussed in detail. The application of ADEPT to a real field case will be detailed in Chapter 8. The application of LBM to predict and simulate asphaltene deposition in porous media based on microchannel experiments has also been examined. More applications of LBM to simulate asphaltene deposition in porous media will be discussed in Chapter 8.

The modeling of asphaltene-transport properties was also presented. Calculations necessary for obtaining density and diffusion coefficient of asphaltenes were described. Modeling methods adopted to predict asphaltene viscosity at particular pressure and temperature conditions, such as, friction theory and CSP models, have also been investigated.

REFERENCES

Abutaqiya, M., J. Zhang, and F. M. Vargas. 2017. Viscosity modeling of reservoir fluids using the friction theory with PC-SAFT crude oil characterization method. *In Preparation*. AQ 6

Akbarzadeh, K., D. Eskin, J. Ratulowski, and S. Taylor. 2012. Asphaltene deposition measurement and modeling for flow assurance of tubings and flow lines. *Energy & Fuels* 26 (1): 495–510. doi:10.1021/ef2009474.

Akbarzadeh, K., J. Ratulowski, T. Lindvig, T. Davis, Z. Huo, and G. Broze. 2009. The importance of asphaltene deposition measurements in the design and operation of subsea pipelines. In *SPE Annual Technical Conference and Exhibition*, pp. 4–7. Retrieved from https://www-onepetro-org.ezproxy.rice.edu/download/conference-paper/SPE-124956-MS?id=conference-paper%2FSPE-124956-MS.

Ali, M. A., and M. R. Islam. 1998. The effect of asphaltene precipitation on carbonate-rock permeability: An experimental and numerical approach. *SPE Production & Facilities* 13 (03): 178–183. doi:10.2118/50963-PA.

Almehaideb, R. A. 2004. Asphaltene precipitation and deposition in the near wellbore region: A modeling approach. *Journal of Petroleum Science and Engineering* 42 (2–4): 157–170. doi:10.1016/j.petrol.2003.12.008.

Andrews, A. B., R. E. Guerra, O. C. Mullins, and P. N. Sen. 2006. Diffusivity of asphaltene molecules by fluorescence correlation spectroscopy. *The Journal of Physical Chemistry A* 110 (26): 8093–8097. doi:10.1021/jp062099n.

Assael, M. J., J. H. Dymond, M. Papadaki, and P. M. Patterson. 1992. Correlation and prediction of dense fluid transport coefficients. I. N-Alkanes. *International Journal of Thermophysics* 13 (2): 269–281.

Barré, L., S. Simon, and T. Palermo. 2008. Solution properties of asphaltenes. *Langmuir* 24 (8): 3709–3717. doi:10.1021/la702611s.

Burger, E. D., T. K. Perkins, and J. H. Striegler. 1981. Studies of wax deposition in the trans alaska pipeline. *Journal of Petroleum Technology* 33 (6): 1075–1086. doi:10.2118/8788-PA.

Carman, P. C. 1939. Permeability of saturated sands, soils and clays. *Journal of Agricultural Science* 29: 263–273. doi:10.1017/S0021859600051789.

Chávez-Miyauchi, T. E., L. S. Zamudio-Rivera, and V. Barba-López. 2013. Aromatic polyisobutylene succinimides as viscosity reducers with asphaltene dispersion capability for heavy and extra-heavy crude oils. *Energy & Fuels* 27 (4): 1994–2001. doi:10.1021/ef301748n.

Chung, T. H., M. Ajlan, L. L. Lee, and K. E. Starling. 1988. generalized multiparameter correlation for nonpolar and polar fluid transport properties. *Industrial & Engineering Chemistry Research* 27 (4): 671–679. doi:10.1021/ie00076a024.

Delbosc, N., J. L. Summers, A. I. Khan, N. Kapur, and C. J. Noakes. 2014. Optimized implementation of the lattice Boltzmann Method on a graphics processing unit towards real-time fluid simulation. *Computers & Mathematics with Applications*, Mesoscopic Methods for Engineering and Science (Proceedings of ICMMES-2012, Taipei, Taiwan, 23–July 27, 2012), 67 (2): 462–475. doi:10.1016/j.camwa.2013.10.002.

Ely, J. F., and H. J. M. Hanley. 1981. Prediction of transport properties. 1. Viscosity of fluids and mixtures. *Industrial & Engineering Chemistry Fundamentals* 20 (4): 323–332.

Eskin, D., J. Ratulowski, K. Akbarzadeh, and S. Pan. 2011. Modelling asphaltene deposition in turbulent pipeline flows. *The Canadian Journal of Chemical Engineering* 89 (3): 421–441.

Eyssautier, J., I. Hénaut, P. Levitz, D. Espinat, and L. Barré. 2012. Organization of asphaltenes in a vacuum residue: A small-angle X-Ray Scattering (SAXS)–Viscosity approach at high temperatures. *Energy & Fuels* 26 (5): 2696–2704. doi:10.1021/ef201412j.

Ferréol, B., and D. H. Rothman. 1995. Lattice-Boltzmann simulations of flow through Fontainebleau sandstone. *Transport in Porous Media* 20 (1): 3–20. doi:10.1007/BF00616923.

Ge, Q., Y. F. Yap, F. M. Vargas, M. Zhang, and J. C. Chai. 2013. Numerical modeling of asphaltene deposition. *Computational Thermal Sciences* 5 (2): 153–163. doi:10.1615/ComputThermalScien.2013006316.

Gruesbeck, C., and R. E. Collins. 1982. Entrainment and deposition of fine particles in porous media. *Society of Petroleum Engineers Journal* 22 (06): 847–856. doi:10.2118/8430-PA.

Guan, Q., Y. F. Yap, A. Goharzadeh, J. Chai, F. M. Vargas, W. Chapman, and M. Zhang. 2017. Integrated one-dimensional modeling of asphaltene deposition in wellbores/pipelines. https://pdfs.semanticscholar.org/664e/797f035562cc521287fb04b5f052a1ffecac.pdf.

Guo, Y., and M. Wang. 2016. Lattice Boltzmann modeling of phonon transport. *Journal of Computational Physics* 315: 1–15. doi:10.1016/j.jcp.2016.03.041.

Guo, Z. 2013. *Lattice Boltzmann Method and Its Applications in Engineering*. Hackensack, NJ: World Scientific Publishing.

Hashmi, S. M., M. Loewenberg, and A. Firoozabadi. 2015. Colloidal asphaltene deposition in laminar pipe flow: Flow rate and parametric effects. *Physics of Fluids* 27 (8): 083302. doi:10.1063/1.4927221.

Haskett, C. E., and M. Tartera. 1965. A practical solution to the problem of asphaltene deposits-Hassi Messaoud Field, Algeria. *Journal of Petroleum Technology* 17 (04): 387–391. doi:10.2118/994-PA.

He, P., Y.-J. Lin, M. Tavakkoli, J. Creek, J. Wang, F. M. Vargas, and S. L. Biswal. 2017. Effect of flow rates on the deposition of asphaltenes in porous media. *In Preparation*.

Heijs, A. W. J., and C. P. Lowe. 1995. Numerical evaluation of the permeability and the Kozeny constant for two types of porous media. *Physical Review E* 51 (5): 4346–4352.

Hirschberg, A., L. N. J. DeJong, B. A. Schipper, and J. G. Meijer. 1984. Influence of temperature and pressure on asphaltene flocculation. *Society of Petroleum Engineers Journal* 24 (03): 283–293. doi:10.2118/11202-PA.

Jafari Behbahani, T., C. Ghotbi, V. Taghikhani, and A. Shahrabadi. 2015. Experimental study and mathematical modeling of asphaltene deposition mechanism in core samples. *Oil & Gas Science and Technology –Revue d'IFP Energies nouvelles* 70 (6): 1051–1074.

Jossi, J. A., L. I. Stiel, and G. Thodos. 1962. The viscosity of pure substances in the dense gaseous and liquid phases. *AIChE Journal* 8 (1): 59–63.

Kord, S., O. Mohammadzadeh, R. Miri, and B. S. Soulgani. 2014. Further investigation into the mechanisms of asphaltene deposition and permeability impairment in porous media using a modified analytical model. *Fuel* 117, Part A: 259–268. doi:10.1016/j.fuel.2013.09.038.

Krieger, I. M., and T. J. Dougherty. 1959. A mechanism for non-newtonian flow in suspensions of rigid spheres. *Transactions of the Society of Rheology* 3 (1): 137–152.

Kurup, A. S., F. M. Vargas, J. Wang, J. S. Buckley, J. L. Creek, J. Subramani, and W. G. Chapman. 2011. Development and application of an asphaltene deposition tool (ADEPT) for well bores. *Energy & Fuels* 25 (10): 4506–4516.

Kurup, A. S., J. Wang, H. J. Subramani, J. S. Buckley, J. L. Creek, and W. G. Chapman. 2012. Revisiting asphaltene deposition tool (ADEPT): Field application. *Energy & Fuels* 26 (9): 5702–5710.

Lawal, K. A., V. Vesovic, and E. S. Boek. 2011. Modeling permeability impairment in porous media due to asphaltene deposition under dynamic conditions. *Energy & Fuels* 25 (12): 5647–5659. doi:10.1021/ef200764t.

Lohrenz, J., B. G. Bray, and C. R. Clark. 1964. Calculating viscosities of reservoir fluids from their compositions. *Journal of Petroleum Technology* 16 (10). doi:10.2118/915-PA.

Maqbool, T., S. Raha, M. P. Hoepfner, and H. Scott Fogler. 2011. Modeling the aggregation of asphaltene nanoaggregates in crude oil-precipitant systems. *Energy & Fuels* 25 (4): 1585–1596.

McNamara, G. R., and G. Zanetti. 1988. Use of the Boltzmann equation to simulate lattice-gas automata. *Physical Review Letters* 61 (20): 2332–2335.

Mehrotra, A. K., W. D. Monnery, and W. Y. Svrcek. 1996. A review of practical calculation methods for the viscosity of liquid hydrocarbons and their mixtures. *Fluid Phase Equilibria* 117: 344–355.

Minssieux, L. 1997. Core damage from crude asphaltene deposition. In SPE: Society of Petroleum Engineers. doi:10.2118/37250-MS.

Mohamad, A. A. 2011. *Lattice Boltzmann Method Fundamentals and Engineering Applications with Computer Codes*. London, UK: Springer.

Mooney, M. 1951. The viscosity of a concentrated suspension of spherical particles. *Journal of Colloid Science* 6 (2): 162–170.

Nit, C., L. M. Itu, and C. Suciu. 2013. GPU accelerated blood flow computation using the Lattice Boltzmann Method. In 1–6. doi:10.1109/HPEC.2013.6670324.

Pal, R., and E. Rhodes. 1989. Viscosity/concentration relationships for emulsions. *Journal of Rheology* 33 (7): 1021. doi:10.1122/1.550044.

Pal, R., and F. Vargas. 2014. On the interpretation of viscosity data of suspensions of asphaltene nano-aggregates. *The Canadian Journal of Chemical Engineering* 92 (3): 573–577. doi:10.1002/cjce.21896.

Pedersen, K. S., P. L. Christensen, and J. A. Shaikh. 2015. *Phase Behavior Of Petroleum Reservoir Fluids*, 2nd Ed. Boca Raton, FL: Taylor & Francis Group.

Pedersen, K. S., A. Fredenslund, P. L. Christensen, and P. Thomassen. 1984. Viscosity of crude oils. *Chemical Engineering Science* 39 (6): 1011–1016.

Premnath, K. N., M. J. Pattison, and S. Banerjee. 2013. An investigation of the lattice Boltzmann method for large eddy simulation of complex turbulent separated flow. *Journal of Fluids Engineering* 135 (5): 051401. doi:10.1115/1.4023655.

Quiñones-Cisneros, S. E., S. I. Andersen, and J. Creek. 2005. Density and viscosity modeling and characterization of heavy oils. *Energy & Fuels* 19 (4): 1314–1318. doi:10.1021/ef0497715.

Quiñones-Cisneros, S. E., C. K. Zéberg-Mikkelsen, and E. H. Stenby. 2000. The friction theory (F-theory) for viscosity modeling. *Fluid Phase Equilibria* 169 (2): 249–276. doi:10.1016/S0378-3812(00)00310-1.

Quiñones-Cisneros, S. E., C. K. Zéberg-Mikkelsen, and E. H. Stenby. 2001. One parameter friction theory models for viscosity. *Fluid Phase Equilibria* 178 (1–2): 1–16. doi:10.1016/S0378-3812(00)00474-X.

Ramirez-Jaramillo, E., C. Lira-Galeana, and O. Manero. 2006. Modeling asphaltene deposition in production pipelines. *Energy & Fuels* 20 (3): 1184–1196. doi:10.1021/ef050262s.

Sarwar, M., and M. R. Islam. 1997. A non-Fickian surface excess model for chemical transport through fractured porous media. *Chemical Engineering Communications* 160 (1): 1–34. doi:10.1080/00986449708936603.

Schmidt, K. A. G., S. E. Quiñones-Cisneros, and B. Kvamme. 2005. Density and viscosity behavior of a north sea crude oil, natural gas liquid, and their mixtures. *Energy & Fuels* 19 (4): 1303–1313. doi:10.1021/ef049774h.

Soulgani, B. S., B. Tohidi, M. Jamialahmadi, and D. Rashtchian. 2011. Modeling formation damage due to asphaltene deposition in the porous media. *Energy & Fuels* 25 (2): 753–761. doi:10.1021/ef101195a.

Soulgani, B. S., D. Rashtchian, B. Tohidi, and M. Jamialahmadi. 2009. Integrated modelling methods for asphaltene deposition in wellstring. *Journal of the Japan Petroleum Institute* 52 (6): 322–331. doi:10.1627/jpi.52.322.

Succi, S., E. Foti, and F. Higuera. 1989. Three-dimensional flows in complex geometries with the lattice Boltzmann method. *EPL* (*Europhysics Letters*) 10 (5): 433.

Tavakkoli, M., V. Taghikhani, M. R. Pishvaie, M. Masihi, S. R. Panuganti, and W. G. Chapman. AQ 7 2013. Investigation of oil-asphaltene slurry rheological behavior. *Journal of Dispersion Science and Technology*, no. just-accepted. doi:10.1080/01932691.2013.834421.

Tham, M. J., and K. E. Gubbins. 1970. Correspondence principle for transport properties of dense fluids. Nonpolar polyatomic fluids. *Industrial & Engineering Chemistry Fundamentals* 9 (1): 63–70.

Uyehara, O. A., and K. M. Watson. 1944. A universal viscosity correlation. *National Petroleum News* 36: R-714-722.

Vargas, F. M., J. L. Creek, and W. G. Chapman. 2010. On the development of an asphaltene deposition simulator. *Energy & Fuels* 24 (4): 2294–2299. doi:10.1021/ef900951n.

Vesovic, V., and W. A. Wakeham. 1989. Prediction of the viscosity of fluid mixtures over wide ranges of temperature and pressure. *Chemical Engineering Science* 44: 2181–2189.

Vesovic, V., J. P. M. Trusler, M. J. Assael, N. Riesco, and S. E. Quiñones-Cisneros. 2014. Dense fluids: Viscosity. In *Experimental Thermodynamics Volume IX: Advances in Transport Properties of Fluids*, M. J. Assael, A. R. H Goodwin, V. Vesovic, and W. A. Wakeham (Eds.). Cambridge, UK: The Royal Society of Chemistry.

Vilas Bôas Fávero, C., A. Hanpan, P. Phichphimok, K. Binabdullah, and H. S. Fogler. 2016. Mechanistic investigation of asphaltene deposition. *Energy & Fuels* 30 (11): 8915–8921. doi:10.1021/acs.energyfuels.6b01289.

Wang, J., J. S. Buckley, and J. L. Creek. 2004. Asphaltene deposition on metallic surfaces. *Journal of Dispersion Science and Technology* 25 (3): 287–298. doi:10.1081/DIS-120037697.

Wang, S., and F. Civan. 2001. Productivity decline of vertical and horizontal wells by asphaltene deposition in petroleum reservoirs. In Society of Petroleum Engineers. doi:10.2118/64991-MS.

Zeberg-Mikkelsen, C. K., S. E. Quiñones-Cisneros, and E. H. Stenby. 2002. Viscosity prediction of natural gas using the friction theory. *International Journal of Thermophysics* 23 (2): 437–454.

Author Query Sheet

Chapter No.: 6

Query No.	Queries	Response
AQ 1	Please check and confirm if Step 5 can be renumbered as Step 7, and Step 6 to Step 8.	
AQ 2	Please confirm if Step 6 is OK here in the sentence "value obtained in…"?	
AQ 3	Wang and Civan reference has 2001 as publication date. Which is correct? Please fix here in table as needed.	
AQ 4	Please add reference Bhatnagar, Gross, and Krook to the list.	
AQ 5	Please update year of publication Abutaqiya et al., if possible.	
AQ 6	Please provide volume number and page range for Abutaqiya et al. (2007) and He et al. (2017).	
AQ 7	Please update Tavakkoli et al. (2013), if possible.	